TgCentrin2 is required for invasion and replication in the human parasite *Toxoplasma gondii*

Jacqueline M. Leung[1], Jun Liu[1*], Laura A. Wetzel[1,2], Ke Hu[1#]*

[1]Department of Biology, Indiana University, Bloomington, IN, 47405, USA

[2]Current address: Department of Molecular and Cellular Biology, University of California, Berkeley, CA, 94720, USA

*: equal contributions

Running title: TgCentrin2 required for parasite invasion and replication

#: Address correspondence to:

Email: kehu@indiana.edu

Abstract

Centrins are EF-hand containing proteins ubiquitously found in eukaryotes and are key components of centrioles/basal bodies as well as certain contractile fibers. We previously identified three centrins in the human parasite *Toxoplasma gondii*, all of which localized to the centrioles. However, one of them, TgCentrin2 (CEN2), is also targeted to ring-shaped structures at the apical and basal ends of the parasite, as well as to multiple annuli at the junction between the apical cap and the rest of the membrane cortex. The role(s) that TgCentrin2 plays in these locations was unknown. Here we report the functional characterization of TgCentrin2 in the parasite lytic cycle. After multiple unsuccessful attempts to knock out or knock down the *TgCentrin2* gene with existing tools, we designed a new conditional knockdown method that combines transcriptional and protein stability control to achieve tight regulation of TgCentrin2 levels in the parasite. We discovered that under knockdown conditions, there was an ordered loss of TgCentrin2 from its four compartments, due to differences in incorporation kinetics and structural inheritance over successive generations. This was correlated with the development of major invasion deficiency at early stages of CEN2 knockdown, and replication defects at later stages. These results indicate that TgCentrin2 is incorporated into multiple cytoskeletal structures to serve distinct functions in *T. gondii* that are required for parasite survival.

INTRODUCTION

Centrin-like proteins were first discovered in the ciliated protozoan *Zoothamnium geniculatum* as a component of the spasmoneme, an organelle that contracts in response to calcium binding (Amos *et al.*, 1975). Subsequently, centrins were found to be components of the centrioles/basal bodies and to play an important role in regulating centrosomal duplication, and flagellar biogenesis and function in the cells of many animals and protozoa (Wright *et al.*, 1985; Sanders and Salisbury, 1994; Salisbury, 1995; Paoletti *et al.*, 1996; Salisbury, 2007).

We previously identified three centrins in *Toxoplasma gondii*, a human parasite that causes devastating toxoplasmic encephalitis in immunocompromised individuals and unprotected fetuses. As with canonical centrins in other systems, TgCentrins 1 and 3 (CEN1 and 3) are predominantly localized to the centrioles. Although TgCentrin2 (CEN2) shares a high degree of sequence similarity with CEN1 and 3 (Figure 1A), its localization is remarkably different (Hu *et al.*, 2006). In addition to the centrioles, ectopic expression of CEN2 tagged with eGFP shows that it is also localized to three other structures: a ring-shaped complex at the apex of the parasite (the preconoidal rings), a capping structure at the basal end (the basal complex), as well as ~5-6 peripheral annuli located approximately one-quarter of a parasite length below the apex (Hu *et al.*, 2006) (Figure 1B). The location of the CEN2 annuli coincides with the boundary between the apical cap and the rest of the parasite membrane cortex, as marked by the ISP proteins (Beck *et al.*, 2010).

Since CEN2 is targeted to four distinct structures, we were interested in understanding what function(s) CEN2 played in them. After many failed attempts with established gene manipulation approaches to delete the *CEN2* gene or downregulate its expression, we knocked down *CEN2* expression in *Toxoplasma* using a dual-regulation approach that combines anhydrotetracycline (ATc)-mediated transcription suppression and ddFKBP-mediated protein degradation. We discovered that CEN2 was depleted from its four locations with different kinetics. The loss of CEN2 from the two more apically located structures, the preconoidal rings and peripheral annuli occurred earlier, followed by significant CEN2 depletion from the centrioles and basal complex. This was correlated with a major inhibition of parasite invasion that appeared at early stages of CEN2 knockdown followed by replication defects that developed at later stages. This suggests that CEN2 is critical for multiple aspects of the parasite lytic cycle and that its associated structures comprise potential targets for anti-parasitic measures.

RESULTS

The localization of CEN2 in eGFP-CEN2 knock-in parasites

In the previous studies, the localization of CEN2 was characterized by ectopic expression. To confirm its localization pattern, we replaced the *CEN2* gene with *eGFP-CEN2* using homologous recombination. The resulting *eGFP-CEN2* knock-in line shows that CEN2 is localized to the preconoidal rings, peripheral annuli, centrioles, and basal

complex (Figure 1B-G), the same pattern as ectopically expressed eGFP-CEN2 (Hu *et al.*, 2006; Hu, 2008). Figure 1C-G includes images of parasites at different stages of cell division – a "born-within" type of replication – during which the cortical cytoskeleton of the daughter parasite is built inside the mother. Of the CEN2 containing structures, replication of the centrioles occurs first (Figure 1D, inset), followed by construction of the preconoidal rings (Figure 1E), and then the peripheral annuli, which appear after the ISP1 cap is assembled (Figure 1F&G). Recruitment of CEN2 to the daughter basal complex becomes evident only at a late stage of daughter assembly (Figure 1G).

Unsuccessful attempts to generate CEN2 knockout and knockdown mutants using several established methods

In the knock-in line, the *eGFP-CEN2* coding sequence and the *HXGPRT* drug selection cassette are flanked with LoxP sites, which allows for the excision of this locus upon transfection with Cre recombinase-expressing plasmids. Indeed, significant loss of eGFP-CEN2 fluorescence was observed in many parasites ~48 h after Cre transfection (Figure 1H). However, numerous attempts for isolating *CEN2* knockout clones failed. We also failed to recover *CEN2* knockout clones using a CRISPR-Cas9 based gene deletion strategy (data not shown), suggesting that the complete loss of *CEN2* results in lethality.

The functions of many presumed essential genes have been characterized using the anhydrotetracycline (ATc)-based knockdown method (Meissner *et al.*, 2001; Meissner *et al.*, 2002; Mital *et al.*, 2005; Huynh and Carruthers, 2006). Therefore, we attempted to regulate *CEN2* expression by generating a line in which the expression of *mAppleFP-CEN2* was driven by the TetO7Sag4 promoter and could be downregulated with ATc, which binds to the tetracycline-inducible transactivator (TATi) to inhibit transcription initiation by the promoter. We found that while the ATc treatment significantly downregulated *mAppleFP-CEN2* expression in the initial passages, the ATc control of *CEN2* expression waned considerably over time (data not shown), indicating that ATc-based transcriptional control alone is not sufficient to maintain robust regulation of *CEN2* expression.

Combining transcriptional and translational controls allow for more robust and stable knockdown of CEN2

To achieve tighter regulation of CEN2 expression, we combined the ATc transcriptional regulation system with translational control. Specifically, the *eGFP-CEN2* knock-in parasites were transfected with a plasmid that contains a *ddFKBP-mAppleFP-CEN2* expression cassette controlled by the TetO7Sag4 promoter, as well as an expression cassette for TATi (*eGFP-CEN2* knock-in: *ddFKBP-mAppleFP-CEN2* cKD parasites, referred to as "*eGFP-CEN2* knock-in:cKD" for simplicity). Upon excision of *eGFP-CEN2* from the endogenous locus by transient Cre recombinase expression, clones (*ddFKBP-mAppleFP-CEN2* cKD parasites, referred to as "cKD" for simplicity) were isolated and maintained in the presence of Shield-1, which binds to and stabilizes the ddFKBP domain, thus blocking degradation of ddFKBP-mAppleFP-CEN2 (Figure 2). The cellular level of ddFKBP-mAppleFP-CEN2 from the TetO7Sag4 promoter therefore can be controlled not only with ATc (regulating transcription), but also with Shield-1, the absence of which leads to proteasome-mediated degradation of the fusion protein

(Banaszynski *et al.*, 2006; Herm-Gotz *et al.*, 2007). Figure 3A shows that ddFKBP-mAppleFP-CEN2 was correctly localized to all of the CEN2-containing structures, and downregulation of ddFKBP-mAppleFP-CEN2 expression was achieved by withdrawing Shield-1 from the culture and adding ATc to a final concentration of 270 nM. To measure the kinetics of CEN2 loss, images of vacuoles that contained two to eight parasites were captured after 12 to 120 h of Shield-1 withdrawal and ATc treatment, and fluorescence signals in the preconoidal rings, peripheral annuli, centriole(s), and basal complex were quantified. Twelve hours after Shield-1 withdrawal and ATc addition, CEN2 localization in the preconoidal rings and annuli became undetectable, in contrast to 47 ± 2% and 63 ± 5% of the starting mAppleFP signal that remained in the centriole(s) and basal complex, respectively (Figure 3A). By 48 hours, the average mAppleFP-CEN2 signal in the centriole and the basal complex further decreased to ~12% of that before downregulation. However, this low level of mAppleFP-CEN2 signal remained detectable in the two structures, even after 120 hours of ATc treatment (Figure 3B). As it is unlikely that a protein can persist for ~15-20 generations of the parasite [The parasite doubling time has been estimated to be ~6-8 hours (Black and Boothroyd, 2000)], this residual signal is likely to reflect a basal level of continuing CEN2 synthesis. We observed a similar ordered loss of eGFP-CEN2 in our attempts to generate *CEN2* knockout mutants using the Cre-LoxP based method (Figure 1H).

The kinetics of CEN2 depletion from the four compartments

As shown in Figure 1D-G, the daughter cortical cytoskeleton is built anew inside the mother during the replication of *Toxoplasma* and other apicomplexan parasites, but a subset of cytoskeletal structures, such as the centrioles, are replicated and inherited from the mother. The kinetics of depletion for a protein component from a structure is therefore affected by the synthesis of new protein, the dissociation and degradation rates of pre-existing protein, "dilution" of a finite amount of protein over successive rounds of cellular replication, as well as whether the structure itself is synthesized *de novo* or inherited from the mother. To determine the effect of structural inheritance in CEN2 depletion from the four compartments during knockdown, cKD parasites maintained in Shield-1 were allowed to invade, Shield-1 was then further maintained, or withdrawn and 270 nM ATc was added to downregulate ddFKBP-mAppleFP-CEN2 for 14 hr. Vacuoles containing a single parasite before or undergoing cytokinesis (*i.e.* before completion of the first round of replication post-invasion) were examined. In contrast to cKD parasites maintained in Shield-1 where the mAppleFP signal was prominent in all CEN2-containing structures (Figure 3C, +Shld1), the ATc-treated parasites assembled daughters with CEN2 that was invariably undetectable in the preconoidal rings and peripheral annuli but prominent in the duplicated and partitioned centrioles (Figure 3C, +ATc). In some instances, the daughters emerged in an orientation that permitted observation of mAppleFP signal still present in the preconoidal rings and peripheral annuli of the disintegrating mother cytoskeleton (Figure 3C, +ATc, bottom row), strongly suggesting that the maternal CEN2 in these structures was not reused to build the corresponding structures in the daughters. Depletion of CEN2 from the peripheral annuli did not affect the localization of ISP1 even after a longer period of ATc treatment (Figure S1A, 120 h +ATc), consistent with the fact that CEN2 recruitment to the annuli during daughter formation occurs after assembly of the ISP1 cap (*c.f.* Figure 1E and F).

CEN2 is critical for the parasite lytic cycle

Toxoplasma is an obligate intracellular parasite. Its dissemination in the host relies on its ability to progress through multiple rounds of the lytic cycle, which consists of host cell invasion, parasite replication, and egress. To determine the impact of the loss of CEN2 on the *Toxoplasma* lytic cycle, we examined the efficiency of the parasite in forming plaques in culture when *CEN2* is knocked down in cKD parasites using a range of ATc concentrations, with different pre-treatment conditions (with Shield-1, no drug, or with ATc for two days) (Figure 4). For all pre-treatment conditions, no plaques were found when cKD parasites were subsequently cultured with an ATc concentration of 68 nM or higher, while the parental strain (*eGFP-CEN2* knock-in:cKD) had comparable plaquing efficiencies under all ATc concentrations tested (0 to 1080 nM). No plaques were observed when the cKD parasites were pre-treated with 270 nM ATc for two days, even when there was no ATc added to the culture medium of the plaque assay itself. This suggested *CEN2* played an important role in the ability of the parasite to progress through multiple rounds of the lytic cycle.

Parasites deficient in CEN2 are significantly impaired in invasion

To determine the underlying cause(s) for the blocked lytic cycle of the *CEN2* knockdown parasites, we examined their ability to invade host cells, using an established two-color, immunofluorescence-based invasion assay. In this assay, the extracellular (non-invaded) and invaded parasites are differentially labeled due to a difference in antibody accessibility (Carey *et al.*, 2004; Mital *et al.*, 2005). Extracellular parasites have the outer surface of their plasma membrane fully exposed, and therefore can be directly labeled by an antibody against a surface antigen (SAG1). On the other hand, parasites that have invaded a host cell can only be labeled after permeabilization. We discovered that after ~16 hours of Shield-1 withdrawal and ATc treatment (a timepoint when CEN2 was nearly completely depleted from the preconoidal rings and peripheral annuli, and partially reduced in the centrioles and basal complex), the invasion efficiency of *CEN2* knockdown parasites was ~30% relative to the wild type (Figure 5A and Table 1). Upon 48 h of CEN2 downregulation, the invasion of *CEN2* knockdown parasites decreased to ~10% that of the wild-type (RHΔ*hx*) parasite (Figure 5B and Table 1).

Parasites deficient in CEN2 are significantly impaired in secretion

Parasite invasion requires the secretion of adhesins from the micronemes, which allows the parasite to attach to and move into the host cell (Carruthers and Sibley, 1997; Carruthers *et al.*, 1999; Huynh *et al.*, 2003; Huynh and Carruthers, 2006). A deficiency in the secretion of these adhesins results in severely impaired host cell invasion. One of the best-studied micronemal adhesins is MIC2 (Huynh *et al.*, 2003; Huynh and Carruthers, 2006), which is secreted together with its binding partner M2AP onto the parasite surface and then cleaved, releasing the MIC2 ectodomain into the supernatant. Upon examining the amount of released ectodomain in the supernatant by western blotting, we discovered that after ~40 hr of *CEN2* knockdown, ethanol stimulated MIC2 secretion (Figure 5C) was partially inhibited. The distribution of micronemal vesicles in these parasites appears to be normal (data not shown), indicating that the *CEN2*-containing structures play a role in the mechanics of secretion rather than the biogenesis of micronemal organelles.

Parasites deficient in CEN2 are significantly impaired in replication after CEN2 is depleted from the centrioles

The centrosome (including the centrioles and the spindle pole) is a critical organelle for cell division, and the basal complex has been shown to be involved in parasite cytokinesis (Heaslip *et al.*, 2010). We therefore examined the impact of CEN2 depletion on parasite replication (Figure 6). As the level of CEN2 decreased due to ATc treatment and Shield-1 withdrawal, an increasing proportion of vacuoles contained parasites that deviated from the more canonical one-to-two division process (Figure 6A). After ~24 hours with ATc treatment, ~11% of the vacuoles have parasites divide or grow abnormally, but parasites in most vacuoles divide normally (Figure 6B &7A-B). At this point, CEN2 had been depleted from the preconoidal rings and peripheral annuli to an undetectable level (Figure 3). We thus propose that the CEN2 pools in the preconoidal rings and peripheral annuli do not play a major role in parasite replication. By ~84 hours of ATc treatment, more than 60% of the vacuoles contained parasites that showed signs of abnormal replication (Figure 6B). In addition to multiple (2+) daughters being assembled in mother parasites (Figure 7C), the parasites were often swollen in size and some had undergone nuclear division without cytokinesis (multiple nuclei but with no daughters) (Figure 7D). Although the kinetics of CEN2 depletion from the centrioles and the basal complex are similar, these replication defects are most likely due to CEN2 depletion from the centrioles, because the presence and appearance of the basal complex marker IAP1 [(Frenal *et al.*, 2014); as marked by an anti-IAP1 antibody, this study] are not significantly affected (Figure S1B-C). We note that in the vacuoles that contained parasites with replication defects, there was considerable variation in the size and cell cycle stage of the parasites, indicating that CEN2 depletion does not affect a specific checkpoint and that the cumulative effect of knockdown is stochastic in nature. Interestingly, the partitioning and inheritance of membrane-bound organelles such as the apicoplast (Figure S1D-E), was not severely perturbed. Although the appearance of the apicoplast is more heterogeneous in misshapen CEN2 knockdown parasites (Figure S1E) when compared to parasites expressing stabilized CEN2 (Figure S1D), almost all of these parasites inherited an apicoplast.

DISCUSSION

In this work, we explore the function of TgCentrin2 (CEN2), a protein that localizes to four different cytoskeletal structures in *Toxoplasma gondii.* Using a dual system that regulates transcription through ATc/TATi and protein stability through Shield-1/ddFKBP, we determined the time course of CEN2 depletion by quantitative fluorescence imaging and used it as a guideline to dissect the functional consequences of CEN2 depletion from the individual structures. We found that CEN2 is depleted to an undetectable level from the preconoidal rings and peripheral annuli much earlier than from the centrioles and basal complex. The ordered depletion of CEN2 from the two sets of structures is linked with the development of defects in two distinct steps of the parasite lytic cycle: invasion and replication. This indicates that CEN2 is recruited to multiple cytoskeletal structures and is required for distinct aspects of parasite physiology.

The dual-regulation system is useful to achieve tight control of genes critical for the parasite lytic cycle

Numerous attempts to generate a knockout mutant of *CEN2* using Cre-LoxP and CRISPR-Cas9 based methods failed. Furthermore, a *CEN2* knockdown line in which *CEN2* downregulation solely relied on transcriptional control with ATc quickly became unresponsive to ATc treatment for unknown reasons. While essentiality cannot be positively proven (*i.e.* essential genes cannot be deleted, but unsuccessful attempts to generate knockout mutants do not prove essentiality), these results suggest that the parasite is highly sensitive to altered *CEN2* expression and that *CEN2* is likely to be essential. By using a dual-regulation system that simultaneously utilizes ATc/TATi to control transcription and Shield-1/ddFKBP to control protein stability, the expression of *CEN2* can be consistently downregulated. Although growth adaptation can still be detected over long-term passage (>3 months), the phenotype is sufficiently stable for analysis as long as care is taken to use low passage cultures. Given that a single conditional regulation technique (*e.g.* ATc-based transcriptional regulation or ddFKBP-based protein degradation) is always "leaky" to some extent, a knockdown strategy that employs orthogonal methods can be useful for characterizing the functions of genes that are otherwise difficult to manipulate.

The kinetics of protein knockdown are affected by structural inheritance through cellular replication

In addition to the half-life of transcripts and their protein products, the kinetics of protein knockdown are affected by structural inheritance through cellular replication. Given that *Toxoplasma* and other apicomplexans divide by building daughters inside the mother, if everything else is equal, components of the cortical cytoskeleton or an organelle regenerated *de novo* with every replication should deplete much faster than those of structures inherited from the mother parasite. For proteins such as CEN2 that are components of multiple structures, this is an important consideration when delineating their functions. For instance, our data indicate that structural inheritance plays an important role in the differential depletion of CEN2 from different structures: the CEN2 populations in the preconoidal rings and peripheral annuli are depleted from these structures much earlier, because these structures are made *de novo* during parasite replication. On the other hand, the CEN2 population in the centrioles persists over many generations after downregulation, because each daughter inherits one pair of the duplicated centrioles from the mother. However, factors other than structural inheritance must also contribute to the differential depletion of CEN2, as the CEN2 population in the basal complex does not fit this pattern. A new basal complex is built for each daughter with every generation (Hu *et al.*, 2006; Hu, 2008), but the depletion of CEN2 from the basal complex follows a trend similar to that of the centrioles rather than the preconoidal rings or peripheral annuli. One possible explanation is that as complete CEN2 removal is lethal, only parasites that still express a small amount of CEN2 protein can survive under -Shield-1/+ATc conditions. Due to differences in binding affinity, the residual CEN2 protein in these parasites is preferentially incorporated into the basal complex and centrioles instead of the preconoidal rings and peripheral annuli.

The role of CEN2 in regulating parasite invasion
The downregulation of CEN2 results in pronounced defects in both parasite invasion and replication. The invasion defect emerged at an early stage of CEN2 knockdown (~16h of ATc treatment and Shield-1 withdrawal) when CEN2 had disappeared from the preconoidal rings and peripheral annuli and partially depleted from the centrioles and the basal complex. While the timing of the depletion suggests that preconoidal rings and peripheral annuli might play an important role in parasite invasion, other pools of CEN2 are almost certainly also involved in invasion. In support of this hypothesis, we found that the invasion efficiency of the parasite decreased from 30% to 10% upon further CEN2 depletion (~16h *vs* 48h of ATc treatment and Shield-1 withdrawal) after it has disappeared from the preconoidal rings and peripheral annuli.

Part of the invasion defect can be explained by the impaired secretion of MIC2, an adhesin that mediates parasite attachment to the host cell. While it is tempting to speculate that some of the CEN2-containing structures (*e.g.* the preconoidal rings and the peripheral annuli) might be contractile structures that gate the release of micronemal contents, we have not been able to detect specific concentrations of MIC2 at these locations before or after CEN2 depletion (data not shown). Since MIC2 secretion is not completely blocked by the depletion of CEN2 and the invasion defect of CEN2 knock-down is more severe than that of the MIC2 knockout mutant (Gras *et al.*, 2017), there are likely other processes affected by CEN2 downregulation that account for its function in invasion. For instance, it would be interesting to know how CEN2 might affect the secretion of moving junction components (the RON proteins) from the rhoptries (Alexander *et al.*, 2005; Lamarque *et al.*, 2011; Tonkin *et al.*, 2011), which are critical for invasion. Unfortunately, while the formation of the moving junction has been demonstrated nicely in invading parasites (Aikawa *et al.*, 1978; Alexander *et al.*, 2005; Lebrun *et al.*, 2005), it is difficult to assess this process in parasites that fail to invade.

The role of CEN2 in regulating parasite replication
CEN2 is a component of centrioles and the depletion of CEN2 from the centrioles correlates with an increase in abnormal parasite replication. The centrosome (including the centrioles and the spindle pole) has been hypothesized to orchestrate daughter construction and organelle biogenesis in *Toxoplasma* (Nishi *et al.*, 2008; Francia and Striepen, 2014; Suvorova *et al.*, 2015). For instance, the majority of parasites in which a centrosomal component, Sfi1, has been knocked down fail to initiate construction of the daughter cytoskeleton (Suvorova *et al.*, 2015). When a temperature sensitive mutant of MAPKL was inactivated at the non-permissive temperature, the parasite generated an abnormally high number of daughters without completion of cytokinesis (Suvorova *et al.*, 2015). The significant depletion of CEN2 from the centrioles results in a heterogeneous population of multi-nucleated (without daughters), multi-daughter (2+), as well as normal looking parasites. This suggests that CEN2 does not seem to control a specific "checkpoint" or coupling point of the regulatory circuit of the cell cycle. However, it is worth noting that in the parasites that survive prolonged (~120 hr) ATc treatment, the CEN2 signal in the centrioles remains detectable, likely because complete CEN2 removal is lethal. Therefore, the consequence of total loss of CEN2 for parasite replication

remains unknown. It would also be of interest to determine if other centrin homologs (*e.g.* CEN1 and 3) found in the centrioles play a redundant role.

The CEN2 containing structures are critical for parasite invasion, replication and survival. Future identification and characterization of structure-specific proteins will facilitate more precise function designation, and aid in the discovery of promising "druggable" targets that lead to multiple points of vulnerability in the parasite.

MATERIALS AND METHODS

T. gondii, host cell cultures, and parasite transfection
Tachyzoite *T. gondii* parasites were maintained by serial passage in confluent human foreskin fibroblast (HFFs, ATCC# SCRC-1041) monolayers as previously described (Roos *et al.*, 1994; Leung *et al.*, 2014; Liu *et al.*, 2016). African green monkey renal epithelial cells (BS-C-1, ATCC# CCL-26) used for the invasion assays and rat aortic smooth muscle cells (A7r5, ATCC# CRL-1444) used for live imaging and immunofluorescence assays were cultured in the same manner as HFFs. The *ddFKBP-mAppleFP-CEN2* cKD ("cKD") parasites were cultured in the presence of 125 nM Shield-1 (a kind gift from Dr. Tom Wandless, Stanford University, Stanford) (Banaszynski *et al.*, 2006) to stabilize its ddFKBP-mAppleFP-CEN2. Downregulation of ddFKBP-mAppleFP-CEN2 was achieved by removal of Shield-1 and incubation in medium supplemented with 270 nM anhydrotetracycline (ATc) (Clontech) unless otherwise noted. *T. gondii* transfections were carried out as previously described (Liu *et al.*, 2013).

Alignment analysis of selected centrin homologs.
Selected centrin homologs were aligned using the MUSCLE program accessed through JalView (v2.8.1, http://www.jalview.org) with default parameters and displayed using the Clustal color scheme.

Cloning of plasmids
Primers used in cloning DNA fragments and for sequencing are listed in Table S1. Genomic DNA (gDNA) fragments were amplified using gDNA template prepared from RH, RHΔ*hx* or RHΔ*ku80*Δ*hx* ("RHΔ*ku80*") parasites ((Fox *et al.*, 2009; Huynh and Carruthers, 2009), a kind gift from Dr. Vern Carruthers, University of Michigan, Ann Arbor, MI) using the Wizard Genomic DNA Purification Kit (Cat# A1120, Promega, Madison, WI) according to the manufacturer's instructions. Similarly, coding sequences (CDS) were amplified using *T. gondii* complementary DNA (cDNA). All DNA fragments generated by PCR were confirmed by sequencing.

pTKO2_II-eGFP-CEN2 (for generation of *eGFP-CEN2* knock-in parasites):
This plasmid was constructed in the pTKO2_II plasmid backbone (Heaslip *et al.*, 2010) designed for replacement of genes in *T. gondii* by homologous recombination. Three fragments were generated and ligated with the pTKO2_II vector backbone using the corresponding sites. The 3'UTR of *CEN2* (TgGT1_250340) was amplified using S1 and

AS1 as primers and RH gDNA as the PCR template, and ligated via the *Nhe*I and *Apa*I sites. The 5'UTR was amplified using S2 and AS2 as primers and RH gDNA as the PCR template, and ligated via the *Not*I and *EcoR*I sites. The *eGFP-CEN2* CDS with a Kozak sequence and flanking *Pme*I and *Rsr*II sites was synthesized (GenScript Inc, NJ) and ligated via the *Pme*I and *Rsr*II sites.

pmin-mCherryFP-CEN2 (intermediate plasmid for cloning pTATi1-TetO7Sag4-ddFKBP-mAppleFP-CEN2, below): This plasmid was constructed by Biomeans Inc (Sugar Land, TX). Briefly, the CEN2 CDS was amplified using primers S3 and AS3 and cloned into pCR-Blunt-II-TOPO (Invitrogen), prior to ligation with the plasmid backbone of pmin-mCherryFP-TgICMAP1 via the *Bam*HI and *Afl*II sites. [pmin-mCherryFP-TgICMAP1 has the same vector backbone as pmin-eGFP-TgICMAP1 (Heaslip *et al.*, 2009) but with mCherryFP in place of eGFP]

pTATi1-TetO7Sag4-ddFKBP-mAppleFP-CEN2 (for generation of *eGFP-TgCEN2* knock-in: cKD and cKD parasites):
To generate pTATi1-TetO7Sag4-ddFKBP-mAppleFP-CEN2, two synthesized DNA or plasmid digestion fragments were generated and ligated with the pTATi1-TetO7Sag4 vector backbone using the corresponding sites. The ddFKBP-mAppleFP fragment features a *Mfe*I restriction site in between the ddFKBP and mAppleFP coding sequences, and was synthesized (GenScript Inc, NJ) and ligated via flanking *Nhe*I-*Bam*HI sites to the *Nhe*I-*Bgl*II sites on the vector backbone. The *CEN2* fragment was derived from the pmin-mCherryFP-CEN2 plasmid and ligated via the flanking *Bam*HI-*Afl*II sites to the *Bgl*II-*Afl*II sites on the vector backbone. The pTATi1-TetO7Sag4 vector backbone was constructed from a four-component HiFi assembly (Cat# E5520, New England Biolabs): 1) the vector backbone, which contains the bacterial origin of replication, beta-lactamase gene for ampicillin resistance, Cre recombinase CDS, and DHFR 3'UTR, was generated from an *Apa*I and *Bmt*I double restriction digest of the plasmid ptub1200bp-mAppleFP-Cre (see below); 2) the TATi1 CDS expression cassette was amplified by PCR using primers S4 and AS4 with the plasmid ptub8-TATi1-HX (a kind gift from Dr. Dominique Soldati-Favre, University of Geneva, Geneva, Switzerland) (Meissner *et al.*, 2002) as the template; 3) the sagCATsag chloramphenicol transferase expression cassette was released from the plasmid ptub1200bp-mAppleFP-Cre by digestion with *Ppu*MI and *Hin*dIII; 4) the ATc-responsive TetO7Sag4 mini-promoter was amplified by PCR using primers S5 and AS5 with the plasmid TetO7Sag4_mycGFP (a kind gift from Dr. Dominique Soldati-Favre, University of Geneva, Geneva, Switzerland) (Meissner *et al.*, 2002) as the template. The ptub1200bp-mAppleFP-Cre plasmid intermediate was constructed by ligating via the *PpuM*I and *Nhe*I sites a truncated tubulin promoter amplified by PCR using primers S6 and AS6 with the plasmid ptub-mAppleFP-TLAP2 (Liu *et al.*, 2016) as the template, and ligating via the *Bgl*II and *Afl*II sites the plasmid backbone ptub-mAppleFP-TLAP2 with the Cre recombinase CDS, as amplified by PCR using primers S7 and AS7 with the plasmid ptub-Cre-EGFP (Heaslip *et al.*, 2010) as the template.

pTKO2_II_mCherryFP-Cre-EGFP (for excision of LoxP-flanked *eGFP-TgCEN2* knock-in expression cassette): This plasmid was constructed by ligating the Cre-EGFP

expression cassette from pmin-Cre-EGFP (Heaslip *et al.*, 2010) with the plasmid backbone of pTKO2_II_mCherryFP (Liu *et al.*, 2013) via the *Not*I and *Apa*I sites.

Generation of knock-in, conditional knockdown, and transgenic parasites
eGFP-CEN2 knock-in parasites:
Approximately 1 x 10^7 RH*Δhx* parasites were electroporated with 50 µg of pTKO2_II-eGFP-CEN2 linearized with *Not*I and selected with 25 µg/mL mycophenolic acid and 50 µg/mL xanthine for four passages, and enriched by FACS for parasites with an intermediate level of eGFP signal to reduce the number of parasites in the population that had not undergone double homologous recombination. Clones were screened by fluorescence light microscopy, and confirmed by diagnostic gDNA PCRs to have the *CEN2* endogenous locus replaced by a LoxP-flanked eGFP-CEN2 expression cassette. One clone was further verified by Southern blotting; this clone was used for the subsequent generation of *eGFP-TgCEN2* knock-in:cKD and cKD parasites.

eGFP-TgCEN2 knock-in:cKD parasites:
The *eGFP-CEN2* knock-in parasites were transfected with 30 µg of pTATi1-TetO7Sag4-ddFKBP-mAppleFP-CEN2 that subsequently integrated multiple times, randomly into the parasite genome after selection with 20 µM chloramphenicol.

cKD parasites:
eGFP-TgCEN2 knock-in:cKD parasites (~1 x 10^7) were electroporated with 20 µg of pTKO2-mCherryFP-Cre-eGFP to excise the knock-in expression cassette between the two LoxP sites, selected with 80 µg/mL of 6-thioxanthine for two passages, and screened for the loss of eGFP-CEN2 fluorescence. Clones were confirmed by diagnostic gDNA PCRs. One clone (clone 10) was further verified by Southern blotting and used in all of the experiments reported here. In the resultant parasite line (cKD), the expression level of ddFKBP-mAppleFP-CEN2 is controlled by anhydrotetracycline and Shield-1. The parasite line was maintained in the presence of 125 nM Shield-1 unless indicated otherwise.

Generation of the rat TgCEN3 and TgIAP1 antibodies
Purified recombinant TgCEN3 (TogoA.00877.a.A1.PS00788) and TgIAP1 (TogoA.17172.a.A1.PW29285) proteins (kind gifts from the Seattle Structural Genomics Center for Infectious Disease, Seattle, WA) were used to inject rats for antibody production (Cocalico Biologicals, Inc) and sera of the immunized animals were harvested for performing the immunofluorescence labeling of TgCEN3 and TgIAP1.

FACS and parasite cloning
Fluorescence activated cell sorting was performed using an AriaII flow cytometer (BD Biosciences, San Jose, CA) driven by FACSDiva software at the Indiana University Bloomington Flow Cytometry Core Facility (Bloomington, IN). To subclone parasites by limiting dilution, 3-25 parasites (depending on the survival rate of specific parasite lines after sorting) with the desired fluorescence profile were sorted per well of a 96-well plate containing confluent HFF monolayers. Wells were screened 7-9 days after sorting for single plaques.

Southern blotting
Southern blotting was performed as previously described (Liu *et al.*, 2013; Liu *et al.*, 2016) with probes synthesized using components based on the NEBlot Phototope Kit (New England BioLabs, Cat# N7550) and detected using components based on the Phototope-Star detection kit (New England BioLabs, Cat# N7020). All *T. gondii* gDNA was prepared from freshly egressed parasites and extracted using the Wizard Genomic DNA Purification kit (Cat# A1120, Promega, Madison, WI).

To probe and detect changes at the *CEN2* genomic locus in the RHΔ*hx* (WT), *eGFP-CEN2* knock-in, *eGFP-CEN2* knock-in:cKD, and cKD parasites, 5 µg of gDNA was digested with *Sca*I. A CDS probe (282 bp) specific for Exon 1 of *CEN2* was amplified from *T. gondii* RHΔ*hx* gDNA using primers S8 and AS8, and used as a template in probe synthesis. A probe specific for the region upstream of the *CEN2* genomic locus (168 bp) was amplified from plasmid pTKO2_II-eGFP-CEN2 using primers S9 and AS9 and used as a template in probe synthesis.

Plaque assay
Plaque assays were performed as previously described with some modifications (Liu *et al.*, 2016). A total of 100, 200 or 500 freshly egressed, pre-treated parasites (see below) was added to each well of a 12-well plate containing a confluent HFF monolayer, and incubated undisturbed for 6-7 days. The pre-treatment medium and corresponding incubation medium were either the regular parasite growth medium, or the medium supplemented with the concentrations of either ATc or Shield-1 as indicated in the text and figure legends. Infected monolayers were then fixed with 3.7% (v/v) formaldehyde at 25°C for 10 min, washed with Dulbecco's phosphate-buffered saline (DPBS), stained with 2% (w/v) crystal violet, 20% (v/v) methanol in DPBS for 15 min, gently rinsed with distilled H_2O and air dried.

Quantification of mAppleFP-CEN2 fluorescence in cKD parasites

a. *Parasite culture and imaging conditions*
T. gondii cultures were grown in the absence or presence of 270 nM ATc for 12, 24, 48, 72, 96 or 120 hours prior to live imaging. Multiple flasks of parasites were coordinated with staggered timing such that a freshly lysed flask was used to inoculate 35-mm dishes (#1.5) with a 20-mm microwell (P35G-1.5-20-C; MatTek) approximately 16 hours prior to imaging. This yielded smaller vacuoles containing 2, 4 or 8 parasites to facilitate imaging each of the four CEN2-containing compartments within the parasite for the quantification of mAppleFP-TgCEN2 signal. The medium in each dish was replaced with pre-warmed, phenol red-free CO_2-independent medium (custom order, SKU#RR060058; Gibco/Life Technologies) prior to imaging. Dishes were imaged in a humidified environmental chamber maintained at 37°C.

Twenty full fields of view (1024 x 1024 pixels) were collected with 2x2 binning for quantitative analysis. For each field of view, a reference differential interference contrast (DIC) image was acquired followed by a 3D stack of three z-slices, spaced 1.0 µm apart, of fluorescence images in the mAppleFP and eGFP channels. Irradiation of

each field of view was minimized to prevent photobleaching and kept consistent to reduce variability in the quantification.

b. *Image analysis*
Image analysis strategies and procedures used here were carried out as previously described in (Murray, 2017). The Semper software package [source code kindly provided by Dr. Owen Saxton (Murray-Edwards College, University of Cambridge, United Kingdom) (Saxton *et al.*, 1979)] was used for image analysis.

c. *Grouping of integrated fluorescence and statistical analysis*
A minimum of twenty vacuoles were quantified per parasite line and drug treatment. Vacuoles containing a smaller number of intracellular parasites (2, 4 or 8 parasites) were used for quantification, and the mAppleFP-CEN2 signal was classified into four groups corresponding to each of the compartments it localizes to in the parasite (preconoidal rings, peripheral annuli, centrioles, and basal complex). All photons/sec measurements shown are per individual structure, per parasite except for the peripheral annuli, which were quantified collectively (*i.e.*, all annuli in one parasite grouped as a single value). Since the basal complexes of parasites tend to cluster within a vacuole, these were quantified collectively for each vacuole and subsequently calculated per parasite, based on the number of parasites observed in the corresponding reference DIC image. Data were analyzed using two-way ANOVA and Dunnett's multiple comparisons tests with GraphPad Prism v7 (La Jolla, CA).

Immunofluorescence assay for intracellular parasites
T. gondii-infected HFF monolayers growing in a 3.5 cm glass-bottom dish were fixed with 3.7% (v/v) formaldehyde in DPBS for 10 min, permeabilized with 0.5% (v/v) Triton X-100 (TX-100) in DPBS for 15 min, blocked in 1% (w/v) BSA in DPBS for 30-60 min, followed by antibody labeling (see below). Dishes were incubated with primary antibodies for 30-60 min followed by incubation with secondary antibodies for 30-60 min unless otherwise noted. Primary antibodies and dilutions used were as follows: rabbit anti-ACP, 1:500 (a kind gift from Dr. David Roos, University of Pennsylvania, Philadelphia, PA and Dr. Geoff McFadden, University of Melbourne, Melbourne, Australia) (Waller *et al.*, 1998); rabbit anti-TgIMC1, 1:1,000 (a kind gift from Dr. Con Beckers, University of North Carolina, Chapel Hill) (Mann and Beckers, 2001); mouse anti-TgISP1, 1:1,000 (a kind gift from Dr. Peter Bradley, University of California, Los Angeles) (Beck *et al.*, 2010); mouse anti-TgMIC2 6D10, 1:1,000 (a kind gift from Dr. Vern Carruthers, University of Michigan, Ann Arbor) (Carruthers *et al.*, 2000); rat anti-CEN3, 1:1,000; and rat anti-IAP1, 1:1,000. Secondary antibodies, all used at 1:1,000 dilution were: goat anti-rabbit IgG Alexa488, 1:1,000 (Cat#A11034, Molecular Probes); goat anti-rabbit IgG Alexa568 (Cat#A11036, Molecular Probes); goat anti-rat IgG Alexa488 (Cat#A11006, Molecular Probes); goat anti-rat IgG Alexa568 (Cat#A11077, Molecular Probes); goat anti-mouse IgG Cy3 (Cat#115-166-003, Jackson ImmunoResearch); and goat anti-mouse IgG Alexa568 (Cat# A11031, Molecular Probes). To stain the nucleus, 4',6-diamidino-2-phenylindole (DAPI) was used at a final concentration of 1 μg/mL. All immunofluorescence labeling steps were performed at room temperature.

Intracellular replication assay
Intracellular replication assays were performed as previously described (Heaslip *et al.*, 2010), except parasites were grown for 12, 24, 36, 60, 72 or 84 hours in medium with no drug supplementation, or with 125 nM Shield-1 (+ Shld1) or with 270 nM ATc (+ ATc). To ensure that the number of parasites in a vacuole was countable, for the last three timepoints (*i.e.*, 60, 72 and 84 hours), parasites were first cultured for 48 hours in T12.5cm^2 flasks in the indicated conditions (medium with no drug, or +Shield-1 or +ATc), released by mechanical disruption of the host cell monolayer, then used to inoculate dishes containing the same medium conditions as the originating flasks, for an additional 12, 24 or 36 hours. At each timepoint, dishes were processed for immunofluorescence as described above, using antibodies for markers of the mother and daughter cortex (TgIMC1), centriole (TgCEN3), basal complex (TgIAP1) and a fluorescent nucleic acid stain (DAPI) to count the number of parasites per vacuole and to assess the percentage of replication defects. The number of parasites per vacuole was determined as 2, 4, 8, ≥16 or "odd" (*i.e.*, where the number of parasites was less than 16, and not an integral power of 2). For Figure 6B, vacuoles with any of the following were considered to have replication defects: an odd number of parasites, enlarged parasites, parasites with multiple nuclei or none at all, and parasites with a single daughter or more than two daughters. Note that for Figure 6C, particularly at the 36 hour and (48+36) hour timepoints, there were many very large vacuoles containing from 16 to upwards of ~128 parasites. However, since the precise number of parasites within each of these vacuoles could not be calculated, they were grouped into the "16 or more parasites" bin and assigned four doublings (four rounds of replication, equivalent to 16 parasites). Therefore, the replication rates for these timepoints are an underestimate of the actual replication rate.

For every timepoint, a minimum of 200 vacuoles were assessed for each parasite line and condition in each of three independent experiments, except for the conditional knockdown parasite line treated with ATc, in which 100 vacuoles were quantified per timepoint because its invasion deficiency resulted in a much lower number of vacuoles formed. Data were analyzed using two-way ANOVA and Bonferroni's multiple comparisons tests with GraphPad Prism v7 (La Jolla, CA). Where statistically significant, multiplicity adjusted P values for comparisons are indicated with asterisks.

Invasion assays
Invasion assays were performed as previously described (Leung *et al.*, 2017) with the following modifications. Since we observed during routine culturing that there was a clear invasion defect for a subset of the parasite lines, preparation of the cultures was adjusted in terms of the amount of inoculum, and timed such that all parasite preparations would be at the same stage, at the time of harvest. For ATc treatment, at approximately 48, 40 or 16 hours prior to harvest, the medium for the indicated subset of parasites was changed to that containing 270 nM ATc and no Shield-1.

The secondary antibody used was changed to rabbit anti-TgSAG1 (a kind gift from Dr. Lloyd Kasper, Dartmouth College, Lebanon, NH) at 1:1000 dilution for 30 min, followed by goat anti-rabbit IgG Alexa488 at 1:1000 dilution for 30 min. The dishes were imaged at low magnification (Olympus 20X UPlanApo, numerical aperture (NA) = 0.70) for a total of 15 full-fields of view per sample for each of three independent experiments. Fields were randomly selected using the Alexa488 channel.

Semi-automated quantification of invaded parasites was performed using FIJI (ImageJ v. 2.0.0-rc-65/1.51s; (Schindelin et al. 2012; Schneider et al. 2012)) as previously described (Leung et al., 2017). Pairwise comparisons were made with unpaired, two-tailed Student's t-tests using GraphPad Prism, v7 (GraphPad, La Jolla, CA).

Microneme secretion (excretory/secretory antigen assay)

Microneme secretion assays were performed as previously described (Leung *et al.*, 2017) with some modifications. Freshly egressed parasites were harvested and resuspended in DMEM supplemented with 1% (v/v) cosmic calf serum (Hyclone, Cat# SH30087.3). Excreted/secreted antigen preparation was performed by incubating 2.3 x 10^7 parasites (adjusting the final volume to 90 µL) at 37°C for 8 min in 2% (v/v) ethanol to assess induced secretion. Tubes were placed on ice for 5 min immediately afterwards, and centrifuged at 1,000 x *g* for 6 min at 4°C. 80 µL of the supernatant was removed and centrifuged again, and 23 µL 4X NuPAGE sample buffer was added to 70 µL of the second supernatant. The pellet was washed with DPBS and resuspended in 2X NuPAGE sample buffer. Samples were boiled for 10 min and resolved using NuPAGE 4-12% Bis-Tris gels, and blotted by wet transfer to nitrocellulose membrane. Membranes were processed for western blotting by probing with mouse mAb anti-TgMIC2 6D10 (1:5,000) and rabbit anti-TgMLC1 (1:2,000; a kind gift from Dr. Con Beckers, University of North Carolina, Chapel Hill) in TBS-T + 5% (w/v) BSA, washed with TBS-T, followed by goat anti-mouse IRDye 680RD and goat anti-rabbit IRDye 800CW infrared dye-conjugated antibodies (1:20,000; LI-COR) in TBS-T + 5% (w/v) nonfat dry milk. Blots were scanned in the 700- and 800-nm channels using an LI-COR Odyssey Classic imaging system (LI-COR Biosciences, Lincoln, NE).

Wide-field deconvolution microscopy

Image stacks were acquired at 37°C using a DeltaVision imaging station (GE Healthcare / Applied Precision) fitted onto an Olympus IX-70 inverted microscope base. A 60X silicone oil immersion lens (Olympus 60X U-Apo N, NA 1.3) used with or without an auxiliary magnification of 1.5X, or 100X oil immersion lens (Olympus 100X UPLS Apo, NA = 1.40) with immersion oil at a refractive index of 1.524 was used for imaging. 3D image stacks were collected with a z-spacing of 0.3 µm unless otherwise noted. Images were deconvolved using the point spread functions and software supplied by the manufacturer. All samples for wide-field deconvolution and for 3D-SIM (below) were prepared in 35-mm dishes (#1.5) with a 20- or 14-mm microwell (P35G-1.5-20-C or P35G-1.5-14-C; MatTek) in phenol red-free, CO_2-independent medium for live imaging and in DPBS + 10 mM sodium azide for fixed samples. Contrast levels were adjusted to better visualize the weak signal without oversaturating the strong signal.

Three-dimensional structured-illumination microscopy (3D-SIM)

3D-SIM image stacks were acquired using an OMX imaging station (GE Healthcare / Applied Precision, Seattle, WA). A 100X oil immersion lens (NA = 1.40) with immersion oil at a refractive index of 1.516 or 1.518 was used; stacks were collected with a z-spacing of 0.125 µm. Images were deconvolved using the point spread functions and software supplied by the manufacturer.

ACKNOWLEDGEMENTS

We thank Dr. Owen Saxton (Murray-Edwards College, University of Cambridge, United Kingdom) for the Semper image processing software, Drs. Con Beckers (University of North Carolina, Chapel Hill) for the rabbit anti-TgIMC1 and anti-TgMLC1 antibodies, Peter Bradley (University of California, Los Angeles) for the mouse anti-TgISP1 antibody, Vern Carruthers (University of Michigan, Ann Arbor) for the RH*Δku80Δhx* parasites and mouse mAb 6D10 anti-TgMIC2 antibody, Richard Day (Indiana University School of Medicine, Indianapolis, IN) for the pmAppleFP-C1 plasmid, Lloyd Kasper (Dartmouth College, Lebanon, NH) for the rabbit anti-TgSAG1 antibody, Dominique Soldati-Favre (University of Geneva, Geneva, Switzerland) for the TetO7Sag4_mycGFP and ptub8-TATi1-HX plasmids, Tom Wandless (Stanford University, Stanford, CA) for Shield-1, David Roos (University of Pennsylvania, Philadelphia, PA) and Geoff McFadden (University of Melbourne, Melbourne, Australia) for the rabbit anti-ACP antibody, and the Seattle Structural Genomics Center for Infectious Disease (Seattle, WA) for the purified recombinant TgCEN3 and TgIAP1. We thank Christiane Hassel of the Indiana University Bloomington (IUB) Flow Cytometry Core Facility for assistance with flow cytometry, and Dr. James Powers of the IUB Light Microscopy Imaging Facility for assistance and support with light microscopy (NIH S10-RR028697). We would also like to thank Dr. Amanda Rollins and Qing Zhang for technical support. This study was supported by American Heart Association Postdoctoral Fellowships (16POST31330004 and 18POST34090005) awarded to J.M.L., and funding from the March of Dimes (6-FY15-198), the National Institutes of Health/National Institute of Allergy and Infectious Diseases (R01-AI098686) awarded to K.H., and facility funding from the Indiana Clinical and Translational Sciences Institute to K.H., funded in part by Grant UL1 TR001108 from a National Institutes of Health, National Center for Advancing Translational Sciences, Clinical and Translational Sciences Award.

FIGURE LEGENDS:

Figure 1. Phylogenetic analysis of selected centrin homologs and the localization of TgCentrin 2 (CEN2) in *Toxoplasma gondii*.

(A) Alignment of TgCentrin1-3 (TgCEN1-3) and selected centrin homologs in other organisms using the multiple alignment program MUSCLE. PfCEN2 (GenBank XP_001348617.1), GnCEN2 XP_011129982.1, TgCEN2 TGGT1_250340, Pt_EFh_containing_protein XP_001441649.1, Ttcaltractin_ICL1d XP_001023350.1b, ScCEN NP_014900.3, AtCEN2 NP_190605.1, CrCEN XP_001699499.1, TgCEN1 TGGT1_247230, HsCEN2 gi|4757902|ref|NP_004335.1, HsCEN1 NP_004057.1, TgCEN3 TGGT1_260670, HsCEN3 NP_004356.2, Pf: *Plasmodium falciparum*; Gn: *Gregarina niphandrodes*; Tg: *Toxoplasma gondii*; Pt: *Paramecium tetraurelia*; Tt: *Tetrahymena thermophila*; Sc: *Saccharomyces cerevisiae*; At: *Arabidopsis thaliana*; Cr: *Chlamydomonas reinhardtii*; Hs: *Homo sapiens*.

(B) Cartoon of an interphase parasite, in which CEN2-containing structures are highlighted in green. Pcr: preconoidal rings; PA: peripheral annuli; C: centrioles; BC: basal complex; AC: apical complex; PM: plasma membrane; IMC: inner membrane complex; Cortical MTs: cortical microtubules.

(C-G) Projections of 3D-SIM images of *eGFP-CEN2* knock-in parasites at different stages of the cell cycle labeled with a mouse anti-ISP1 antibody. Insets (2X) in C, D, and F are contrast enhanced and include regions indicated by the arrows. Dashed lines in C, D, and G indicate the approximate outline of one of the two parasites in the same vacuole. The cartoon in G highlights the localization of CEN2 and ISP1 with respect to the inner membrane complex (IMC) and the plasma membrane. M-Pcr: mother preconoidal rings; D-Pcr: daughter preconoidal rings; D-PA: peripheral annuli; M-IMC: mother IMC; D: daughter. Other abbreviations are the same as in (B). Green: eGFP-CEN2; Red: anti-ISP1. Scale bar = 2 µm.

(H) Fluorescence (top) and fluorescence/DIC overlay (bottom) images of *eGFP-CEN2* knock-in parasites ~48 h after transfection with a plasmid expressing Cre recombinase. There are two vacuoles in the field. Dashed circles indicate the vacuole in which eGFP-CEN2 expression has decreased significantly. Inset (1X) is contrast enhanced to visualize residual eGFP-CEN2 signal in the centrioles (arrows) and basal complex (arrowheads) of the parasites in this vacuole. Scale bar = 5 µm.

Figure 2. Generation of the knock-in and cKD parasite lines

(A) Schematic for generating *eGFP-CEN2* knock-in, *eGFP-CEN2* knock-in:cKD and cKD parasites and Southern blotting strategy. Positions of the *Sca*I restriction sites, CDS probe (blue) and the probe annealing upstream of the *CEN2* coding sequence (5'UTR probe, red) used in the Southern blotting analysis and the corresponding DNA fragment sizes expected are indicated as shown.
(B) Southern blotting analysis of the *CEN2* locus in RHΔ*hx* parasites (WT), *eGFP-CEN2* knock-in (KI), *eGFP-CEN2*:cKD (KI:cKD) and cKD parasites. For the CDS probe, the expected parasite genomic DNA fragment sizes after *Sca*I digestion are 8696 base pairs for the parental (*i.e.*, wild-type *CEN2* locus), 10,630 base pairs for the knock-in, and

variable for the multiple, random integrations of the cKD plasmid (pTATi1-TetO7Sag4-ddFKBP-mAppleFP-CEN2) since the fragment sizes would depend on where the plasmid integrated relative to *Sca*I sites in the parasite genome. The expected DNA fragment sizes for the upstream probe are the same as for the CDS probe for the parental and knock-in, and 6960 base pairs for the knock out. L: ladder.

Figure 3. Quantification of CEN2 downregulation in cKD parasites over 120 hours. (A) Representative fluorescence and DIC images of cKD parasites in two to four parasite vacuoles cultured in the presence of Shield-1 (+Shld1), or 12, 24, and 48 h after withdrawal of Shield-1 and addition of ATc (+ATc). The image of the vacuole at 48 h with ATc is representative of vacuoles imaged at subsequent timepoints (72, 96, and 120 h). All images in each row were acquired and processed under the same conditions. Images in the middle row were highly contrast enhanced to display low mAppleFP-CEN2 signal in the parasites. Scale bar = 2 µm.

(B) Graph shows the intensity measurements of mAppleFP-CEN2 in the preconoidal rings (red), peripheral annuli (orange), centrioles (green) and basal complex (blue), showing that CEN2 is depleted from the preconoidal rings and peripheral annuli much earlier than from the centrioles and basal complex. All values compared to the baseline (cKD parasites cultured in Shield-1 and without ATc) had multiplicity adjusted P values of less than 0.0001 except for the basal complex at T=12 h. Note that the two segments of the y-axis are scaled differently to facilitate better visualization of the lower photon counts in the later timepoints. Error bars: standard error of the mean.

(C) Fluorescence images of cKD parasites in the presence of Shield-1 or treated for 14 h with ATc and no Shield-1, in single parasite vacuoles before or undergoing the first round of cytokinesis post-invasion. Dashed circles indicate daughters emerging from the mother parasite. The arrow indicates the preconoidal rings and peripheral annuli in the disintegrating maternal cytoskeleton. Scale bar = 2 µm.

Figure 4. The effect of CEN2 downregulation on the parasite lytic cycle.

Plaques formed in the presence of 0 nM, 68 nM, 135 nM, 270 nM, 540 nM and 1080 nM ATc and without Shield-1 by the *eGFP-CEN2* knock-in:cKD (Parental) and cKD parasites. "Pre-treat": The cKD parasites were pre-treated for ~48 h with 125 nM Shield-1 (Shld1), no drug, or 270 nM ATc. Each well of HFF monolayers was infected with 100 parasites, grown for 6 days at 37°C, and then fixed and stained with crystal violet. Host cells that remained intact absorbed the crystal violet staining, whereas regions of host cells lysed by the parasites ("plaques") are clear.

Figure 5. The effect of CEN2 downregulation on parasite invasion and secretion.

(A) and (B) Representative wide-field epifluorescence images of invasion by RHΔ*hx* parasites (WT), *eGFP-CEN2*:cKD (KI:cKD) and cKD parasites with 125 nM Shield-1 (Shld1), no drug, or 270 nM ATc as indicated. Parasites that are intracellular (*i.e.*, have successfully invaded) are labeled green, and parasites that did not invade are labeled both green and red (*i.e.* appear yellow). See Table 1 for quantification of the invasion

efficiency (mean ± standard error) relative to WT parasites, as measured in three independent biological replicates. Scale bar = 20 µm.

(C) The unsecreted (pellet) and secreted (supernatant) fractions of *eGFP-CEN2* knock-in:cKD (KI:cKD, no drug or +ATc) and cKD (cKD, +Shld1 or +ATc) parasites upon ethanol stimulation, as probed by antibodies against MIC2, with MLC1 as a loading control. The pellet fraction contains the full-length and the supernatant contains the shed ectodomain of MIC2. The numbers on the left indicate molecular masses in kDa.

Figure 6. The effect of CEN2 downregulation on parasite replication.

(A) Comparison of the intracellular growth of cKD parasites treated with 270nM ATc (cKD+ATc) with that of RH*Δhx* (WT), *eGFP-CEN2* knock-in: cKD (KI:cKD, no drug or +ATc) and cKD parasites cultured in Shield-1 (cKD+Shld1) parasites at 12, 24, 36, 60, 72, and 84 h after drug removal/addition. To facilitate parasite counting after extended (>48 h) drug treatment times, dishes for the last three timepoints were inoculated with parasites that had been cultured for 48 hours in T12.5cm^2 flasks under the indicated conditions, and allowed to invade a fresh HFF monolayer and proliferate for 12, 24, and 36 hours under the corresponding conditions. "Odd", vacuoles in which the number of parasites was less than 16, and not an integral power of 2. "≥16", vacuoles that contained 16 or more parasites.
(B) Percentage of vacuoles containing parasites with replication defects. Phenotypes include an odd number of parasites, enlarged parasites, parasites with multiple nuclei or none at all, and parasites with a single daughter or more than two daughters.
(C) Mean replication (doubling) rate. Error bars: standard error of the mean. **: P values less than 0.01, and ****: P values less than 0.0001 (two-way ANOVA and Bonferroni's multiple comparisons test), when cKD parasites are compared with RH*Δhx* (WT) or *KI:* cKD parasites as measured in three independent biological replicates. Note that particularly at the 36 hour and (48+36) hour timepoints, there were many very large vacuoles containing from 16 to upwards of ~128 parasites. However, since the precise number of parasites within each of these large vacuoles could not be calculated, they were grouped into the "16 or more parasites" bin and assigned four doublings (four rounds of replication, equivalent to 16 parasites). Therefore, the replication rates for these timepoints are an underestimate of the actual replication rate.

Figure 7. CEN2 knockdown results in multiple types of replication defects.
(A) Representative images of untreated RH*Δhx* parasites (WT) at the 24 h timepoint of the replication assays in Figure 6.
(B) Images of a vacuole of cKD parasites treated with 270 nM ATc for 24 h undergoing normal replication.
(C&D) Images of one vacuole of cKD parasites treated with 270 nM ATc for 84 h with more than two daughters forming inside the mother (C, arrowheads) and another vacuole with parasites that are swollen with large or multiple nuclei (D, arrows)
TgCentrin3 (CEN3), marker for the centrioles; TgIMC1 (IMC1), marker for the cortex of mature and daughter parasites; DAPI, marker for the nucleus. Scale bar = 2 µm.

Table 1. Quantification of invasion [mean number of intracellular parasites ± standard error of the mean (SE)] by RHΔ*hx* parasites (WT), *eGFP-CEN2:cKD* (KI:cKD) and *cKD* (cKD) parasites with 125 nM Shield-1 (Shld1), no drug, or 270 nM ATc as indicated. See also Figure 5 for details. The number of intracellular parasites per field was counted in 15 fields per parasite line or treatment, in each of three independent biological replicates. *p* values from unpaired, two-tailed Student's *t* tests are indicated on the right.

Supplemental Figure 1.

Representative images of cKD parasites treated with 125 nM Shield-1 (Shld1) or with 270 nM ATc and labeled with antibodies for (A) ISP1 at 120 h +ATc, IAP1 at 84 h +Shld1 (B) or +ATc (C), and ACP at 87 h +Shld1 (D) or +ATc (E). TgISP1 (ISP1), marker for the apical cap; TgIMC1 (IMC1), marker for the cortex of mature and daughter parasites; IMC associated protein 1(IAP1), marker for the basal complex; acyl carrier protein (ACP), marker for the apicoplast, an inherited, membrane-bound organelle. Scale bar = 2 μm.

Supplemental Table S1. Primers used in this study.

REFERENCES

Aikawa, M., Miller, L.H., Johnson, J., and Rabbege, J. (1978). Erythrocyte entry by malarial parasites. A moving junction between erythrocyte and parasite. J Cell Biol *77*, 72-82.
Alexander, D.L., Mital, J., Ward, G.E., Bradley, P., and Boothroyd, J.C. (2005). Identification of the moving junction complex of Toxoplasma gondii: a collaboration between distinct secretory organelles. PLoS Pathog *1*, e17.
Amos, W.B., Routledge, L.M., and Yew, F.F. (1975). Calcium-binding proteins in a vorticellid contractile organelle. J Cell Sci *19*, 203-213.
Banaszynski, L.A., Chen, L.C., Maynard-Smith, L.A., Ooi, A.G., and Wandless, T.J. (2006). A rapid, reversible, and tunable method to regulate protein function in living cells using synthetic small molecules. Cell *126*, 995-1004.
Beck, J.R., Rodriguez-Fernandez, I.A., Cruz de Leon, J., Huynh, M.H., Carruthers, V.B., Morrissette, N.S., and Bradley, P.J. (2010). A novel family of *Toxoplasma* IMC proteins displays a hierarchical organization and functions in coordinating parasite division. PLoS Pathog *6*.
Black, M.W., and Boothroyd, J.C. (2000). Lytic cycle of Toxoplasma gondii. Microbiol Mol Biol Rev *64*, 607-623.
Carey, K.L., Westwood, N.J., Mitchison, T.J., and Ward, G.E. (2004). A small-molecule approach to studying invasive mechanisms of *Toxoplasma gondii*. Proc Natl Acad Sci U S A *101*, 7433-7438.
Carruthers, V.B., Giddings, O.K., and Sibley, L.D. (1999). Secretion of micronemal proteins is associated with *Toxoplasma* invasion of host cells. Cell Microbiol *1*, 225-235.
Carruthers, V.B., Sherman, G.D., and Sibley, L.D. (2000). The *Toxoplasma* adhesive protein MIC2 is proteolytically processed at multiple sites by two parasite-derived proteases. J Biol Chem *275*, 14346-14353.
Carruthers, V.B., and Sibley, L.D. (1997). Sequential protein secretion from three distinct organelles of *Toxoplasma gondii* accompanies invasion of human fibroblasts. Eur J Cell Biol *73*, 114-123.
Fox, B.A., Ristuccia, J.G., Gigley, J.P., and Bzik, D.J. (2009). Efficient gene replacements in *Toxoplasma gondii* strains deficient for nonhomologous end joining. Eukaryotic cell *8*, 520-529.
Francia, M.E., and Striepen, B. (2014). Cell division in apicomplexan parasites. Nat Rev Microbiol *12*, 125-136.
Frenal, K., Marq, J.B., Jacot, D., Polonais, V., and Soldati-Favre, D. (2014). Plasticity between MyoC- and MyoA-glideosomes: an example of functional compensation in Toxoplasma gondii invasion. PLoS Pathog *10*, e1004504.
Gras, S., Jackson, A., Woods, S., Pall, G., Whitelaw, J., Leung, J.M., Ward, G.E., Roberts, C.W., and Meissner, M. (2017). Parasites lacking the micronemal protein MIC2 are deficient in surface attachment and host cell egress, but remain virulent in vivo. Wellcome Open Res *2*, 32.
Heaslip, A.T., Dzierszinski, F., Stein, B., and Hu, K. (2010). TgMORN1 is a key organizer for the basal complex of *Toxoplasma gondii*. PLoS Pathog *6*, e1000754.
Heaslip, A.T., Ems-McClung, S.C., and Hu, K. (2009). TgICMAP1 is a novel microtubule binding protein in *Toxoplasma gondii*. PloS one *4*, e7406.

Heaslip, A.T., Nishi, M., Stein, B., and Hu, K. (2011). The Motility of a Human Parasite, *Toxoplasma gondii*, Is Regulated by a Novel Lysine Methyltransferase. PLoS Pathog *7*, e1002201.
Herm-Gotz, A., Agop-Nersesian, C., Munter, S., Grimley, J.S., Wandless, T.J., Frischknecht, F., and Meissner, M. (2007). Rapid control of protein level in the apicomplexan *Toxoplasma gondii*. Nat Methods *4*, 1003-1005.
Hu, K. (2008). Organizational changes of the daughter basal complex during the parasite replication of *Toxoplasma gondii*. PLoS Pathog *4*, e10.
Hu, K., Johnson, J., Florens, L., Fraunholz, M., Suravajjala, S., Dilullo, C., Yates, J., Roos, D.S., and Murray, J.M. (2006). Cytoskeletal Components of an Invasion Machine-The Apical Complex of *Toxoplasma gondii*. PLoS Pathog *2*, e13.
Huynh, M.H., and Carruthers, V.B. (2006). *Toxoplasma* MIC2 is a major determinant of invasion and virulence. PLoS Pathog *2*, e84.
Huynh, M.H., and Carruthers, V.B. (2009). Tagging of endogenous genes in a *Toxoplasma gondii* strain lacking Ku80. Eukaryotic cell *8*, 530-539.
Huynh, M.H., Rabenau, K.E., Harper, J.M., Beatty, W.L., Sibley, L.D., and Carruthers, V.B. (2003). Rapid invasion of host cells by *Toxoplasma* requires secretion of the MIC2-M2AP adhesive protein complex. EMBO J *22*, 2082-2090.
Lamarque, M., Besteiro, S., Papoin, J., Roques, M., Vulliez-Le Normand, B., Morlon-Guyot, J., Dubremetz, J.F., Fauquenoy, S., Tomavo, S., Faber, B.W., Kocken, C.H., Thomas, A.W., Boulanger, M.J., Bentley, G.A., and Lebrun, M. (2011). The RON2-AMA1 interaction is a critical step in moving junction-dependent invasion by apicomplexan parasites. PLoS Pathog *7*, e1001276.
Lebrun, M., Michelin, A., El Hajj, H., Poncet, J., Bradley, P.J., Vial, H., and Dubremetz, J.F. (2005). The rhoptry neck protein RON4 re-localizes at the moving junction during Toxoplasma gondii invasion. Cell Microbiol *7*, 1823-1833.
Leung, J.M., He, Y., Zhang, F., Hwang, Y.C., Nagayasu, E., Liu, J., Murray, J.M., and Hu, K. (2017). Stability and function of a putative microtubule-organizing center in the human parasite Toxoplasma gondii. Mol Biol Cell *28*, 1361-1378.
Leung, J.M., Rould, M.A., Konradt, C., Hunter, C.A., and Ward, G.E. (2014). Disruption of TgPHIL1 Alters Specific Parameters of Toxoplasma gondii Motility Measured in a Quantitative, Three-Dimensional Live Motility Assay. PloS one *9*, e85763.
Liu, J., He, Y., Benmerzouga, I., Sullivan, W.J., Jr., Morrissette, N.S., Murray, J.M., and Hu, K. (2016). An ensemble of specifically targeted proteins stabilizes cortical microtubules in the human parasite Toxoplasma gondii. Mol Biol Cell *27*, 549-571.
Liu, J., Wetzel, L., Zhang, Y., Nagayasu, E., Ems-McClung, S., Florens, L., and Hu, K. (2013). Novel thioredoxin-like proteins are components of a protein complex coating the cortical microtubules of Toxoplasma gondii. Eukaryotic cell.
Mann, T., and Beckers, C. (2001). Characterization of the subpellicular network, a filamentous membrane skeletal component in the parasite *Toxoplasma gondii*. Molecular and biochemical parasitology *115*, 257-268.
Meissner, M., Brecht, S., Bujard, H., and Soldati, D. (2001). Modulation of myosin A expression by a newly established tetracycline repressor-based inducible system in Toxoplasma gondii. Nucleic Acids Res *29*, E115.
Meissner, M., Schluter, D., and Soldati, D. (2002). Role of *Toxoplasma gondii* myosin A in powering parasite gliding and host cell invasion. Science *298*, 837-840.

Mital, J., Meissner, M., Soldati, D., and Ward, G.E. (2005). Conditional expression of *Toxoplasma gondii* apical membrane antigen-1 (TgAMA1) demonstrates that TgAMA1 plays a critical role in host cell invasion. Mol Biol Cell *16*, 4341-4349.
Murray, J.M. (2017). An icosahedral virus as a fluorescent calibration standard: a method for counting protein molecules in cells by fluorescence microscopy. J Microsc *267*, 193-213.
Nishi, M., Hu, K., Murray, J.M., and Roos, D.S. (2008). Organellar dynamics during the cell cycle of *Toxoplasma gondii*. J Cell Sci *121*, 1559-1568.
Paoletti, A., Moudjou, M., Paintrand, M., Salisbury, J.L., and Bornens, M. (1996). Most of centrin in animal cells is not centrosome-associated and centrosomal centrin is confined to the distal lumen of centrioles. J Cell Sci *109 (Pt 13)*, 3089-3102.
Roos, D.S., Donald, R.G., Morrissette, N.S., and Moulton, A.L. (1994). Molecular tools for genetic dissection of the protozoan parasite *Toxoplasma gondii*. In: Methods in Cell Biology, vol. 45, 27-63.
Salisbury, J.L. (1995). Centrin, centrosomes, and mitotic spindle poles. Curr Opin Cell Biol *7*, 39-45.
Salisbury, J.L. (2007). A mechanistic view on the evolutionary origin for centrin-based control of centriole duplication. J Cell Physiol *213*, 420-428.
Sanders, M., and Salisbury, J. (1994). Centrin plays an essential role in microtubule severing during flagellar excision in Chlamydomonas reinhardtii. The Journal of Cell Biology *124*, 795-805.
Saxton, W., Pitt, T., and Horner, M. (1979). Digital image processing: the Semper system. Ultramicroscopy *4*, 343-353.
Suvorova, E.S., Francia, M., Striepen, B., and White, M.W. (2015). A novel bipartite centrosome coordinates the apicomplexan cell cycle. PLoS Biol *13*, e1002093.
Tonkin, M.L., Roques, M., Lamarque, M.H., Pugniere, M., Douguet, D., Crawford, J., Lebrun, M., and Boulanger, M.J. (2011). Host cell invasion by apicomplexan parasites: insights from the co-structure of AMA1 with a RON2 peptide. Science *333*, 463-467.
Waller, R.F., Keeling, P.J., Donald, R.G., Striepen, B., Handman, E., Lang-Unnasch, N., Cowman, A.F., Besra, G.S., Roos, D.S., and McFadden, G.I. (1998). Nuclear-encoded proteins target to the plastid in Toxoplasma gondii and Plasmodium falciparum. Proc Natl Acad Sci U S A *95*, 12352-12357.
Wright, R.L., Salisbury, J., and Jarvik, J.W. (1985). A nucleus-basal body connector in Chlamydomonas reinhardtii that may function in basal body localization or segregation. The Journal of Cell Biology *101*, 1903-1912.

Table 1

			P value					
Strain	Number invaded ± SE	% WT	RHΔhx (WT)		cKD, +16 h ATc		cKD, +40 h ATc	
RHΔhx (WT)	103 ± 12	100			0.009		0.0019	
cKD, +16 h ATc	31 ± 10	30					0.2118	
cKD, +40 h ATc	16 ± 1	16						
			P value					
Strain	Number invaded ± SE	% WT	RHΔhx (WT)	KI:cKD, no drug	KI:cKD, +48 h ATc	cKD, +Shld1	cKD, no drug	cKD, +48 h ATc
RHΔhx (WT)	103 ± 12	100		0.1208	0.4845	0.033	0.0071	0.0014
KI:cKD, no drug	129 ± 6	125			0.4163	0.0021	0.0007	0.0001
KI:cKD, +48 h ATc	117 ± 13	113				0.0171	0.0046	0.0011
cKD, +Shld1	58 ± 8	56					0.0756	0.005
cKD, no drug	29 ± 9	28						0.1119
cKD, +48 h ATc	11 ± 2	10						

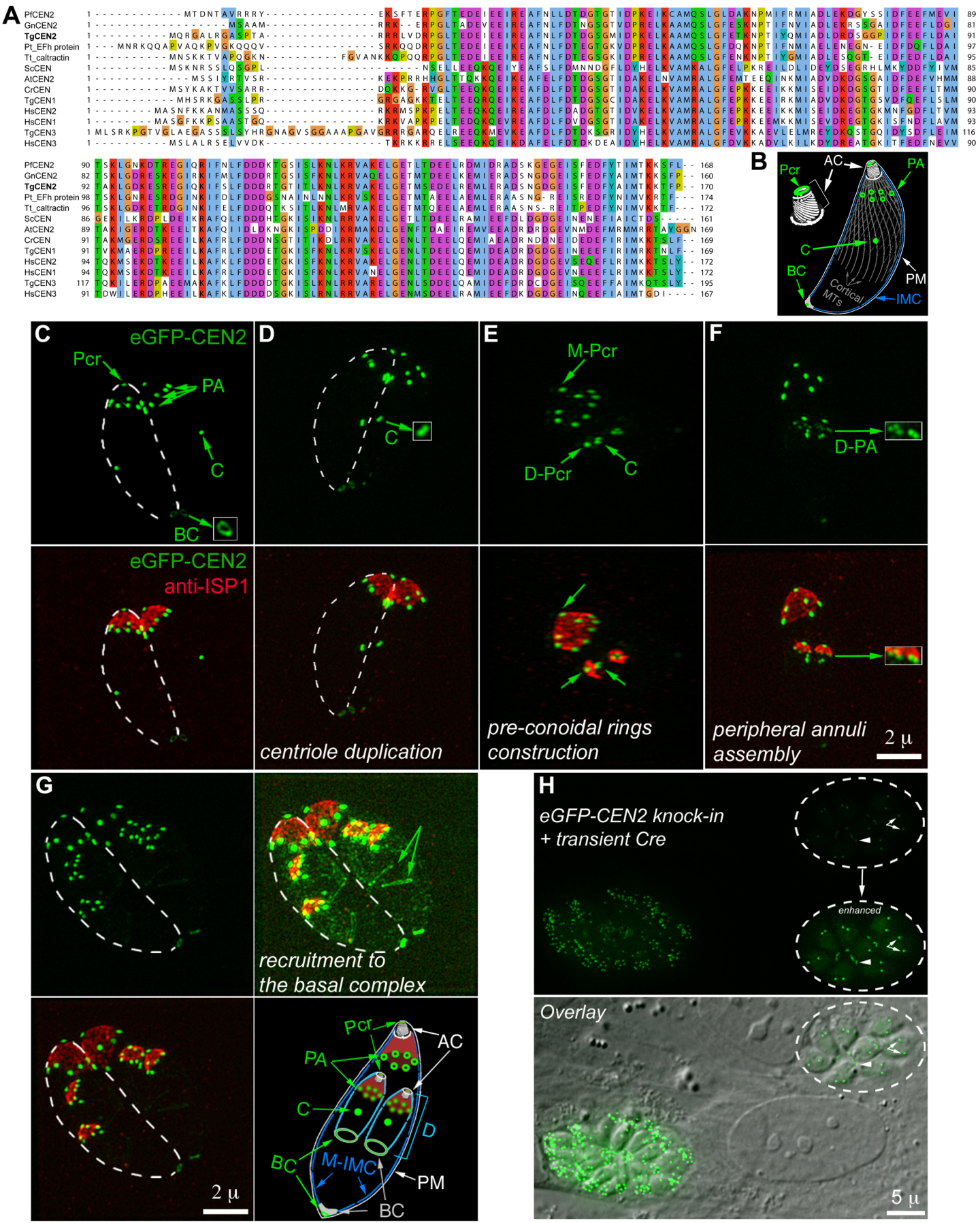
A
PfCEN2
GnCEN2
TgCEN2
Pt_EFh protein
Tt_caltractin
ScCEN
AtCEN2
CrCEN
TgCEN1
HsCEN2
HsCEN1
TgCEN3
HsCEN3
B
Pcr
AC
PA
C
BC
PM
Cortical MTs
IMC
C
eGFP-CEN2
Pcr
PA
C
BC
D
C
E
M-Pcr
D-Pcr
C
F
D-PA
eGFP-CEN2
anti-ISP1
centriole duplication
pre-conoidal rings construction
peripheral annuli assembly
2 µ
G
recruitment to the basal complex
2 µ
Pcr
AC
PA
C
D
BC
M-IMC
PM
BC
H
eGFP-CEN2 knock-in + transient Cre
enhanced
Overlay
5 µ

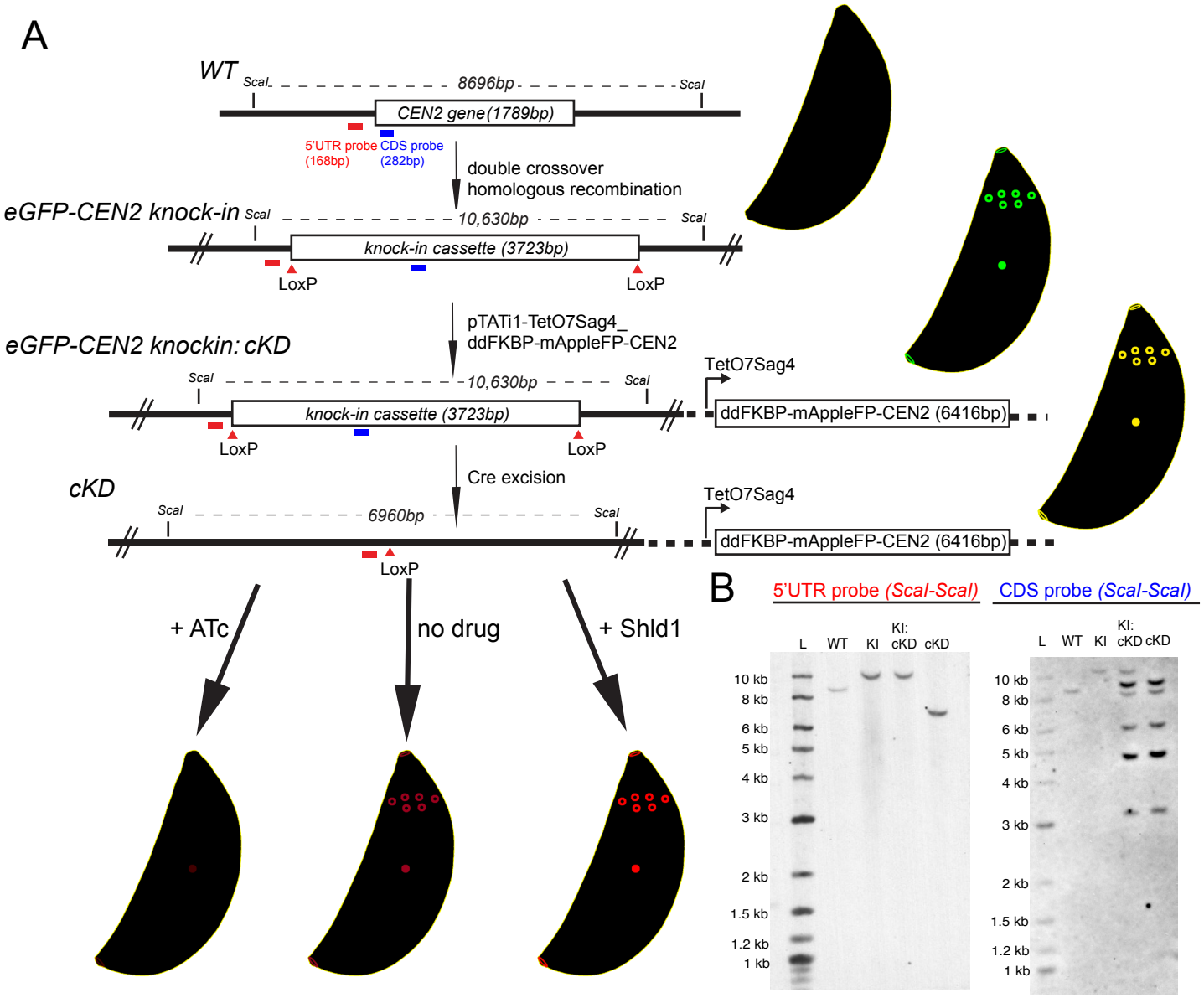
A
WT
ScaI
8696bp
ScaI
CEN2 gene(1789bp)
5'UTR probe (168bp)
CDS probe (282bp)
double crossover homologous recombination
eGFP-CEN2 knock-in
ScaI
10,630bp
ScaI
knock-in cassette (3723bp)
LoxP
LoxP
pTATi1-TetO7Sag4_ ddFKBP-mAppleFP-CEN2
eGFP-CEN2 knockin: cKD
ScaI
10,630bp
ScaI
TetO7Sag4
knock-in cassette (3723bp)
ddFKBP-mAppleFP-CEN2 (6416bp)
LoxP
LoxP
Cre excision
cKD
ScaI
6960bp
ScaI
TetO7Sag4
ddFKBP-mAppleFP-CEN2 (6416bp)
LoxP
+ ATc
no drug
+ Shld1
B
5'UTR probe (ScaI-ScaI)
CDS probe (ScaI-ScaI)
L
WT
KI
KI: cKD
cKD
10 kb
8 kb
6 kb
5 kb
4 kb
3 kb
2 kb
1.5 kb
1.2 kb
1 kb

Figure 2

Figure 3

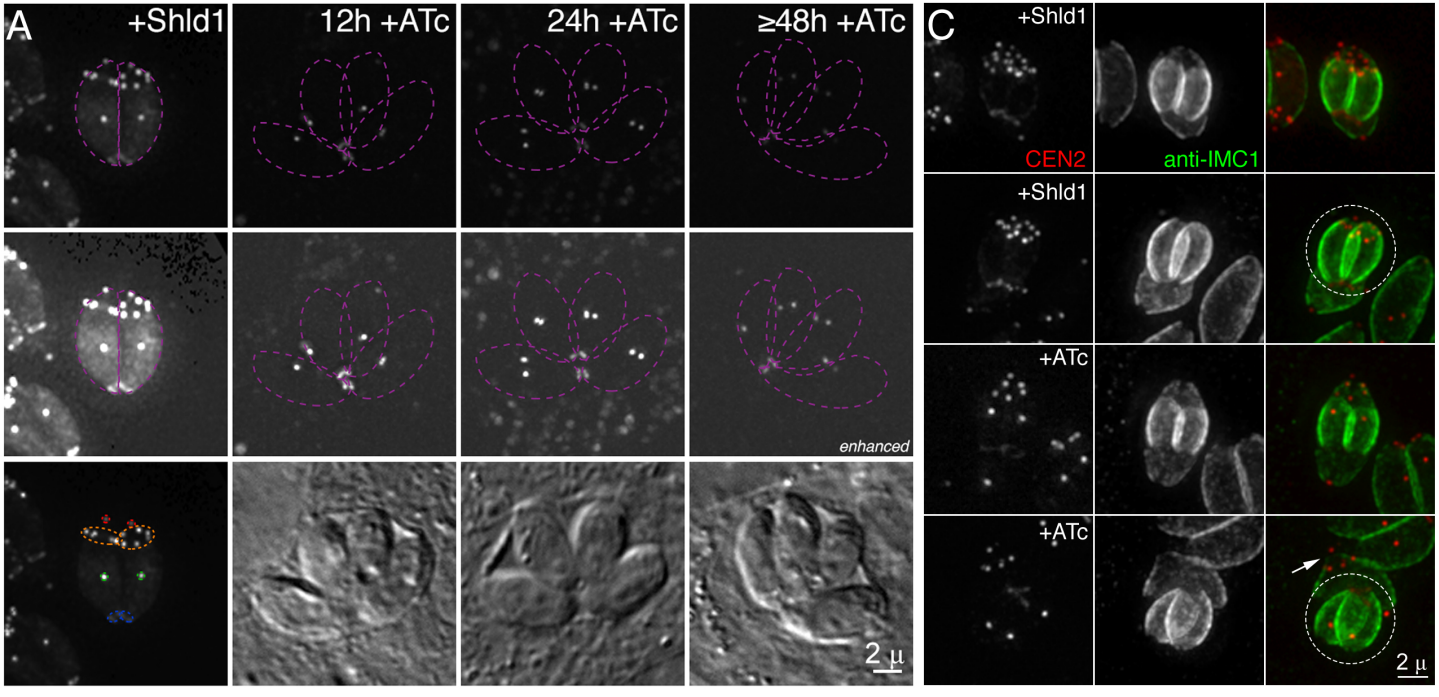
A
+Shld1
12h +ATc
24h +ATc
≥48h +ATc
enhanced
2 µ
C
+Shld1
CEN2
anti-IMC1
+Shld1
+ATc
+ATc
2 µ

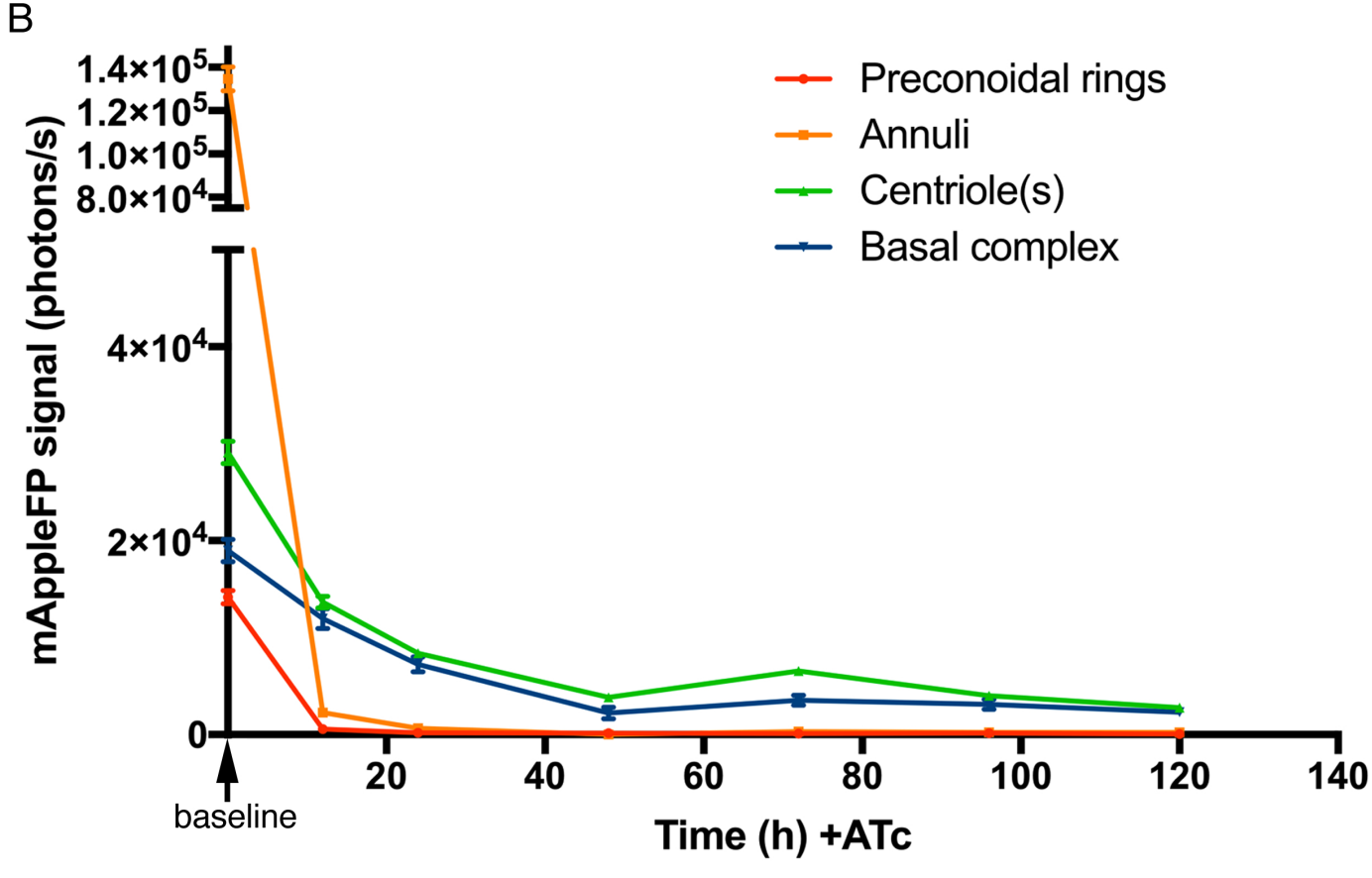
B
Preconoidal rings
Annuli
Centriole(s)
Basal complex
mAppleFP signal (photons/s)
1.4×10^5
1.2×10^5
1.0×10^5
8.0×10^4
4×10^4
2×10^4
0
20
40
60
80
100
120
140
baseline
Time (h) +ATc

Figure 4

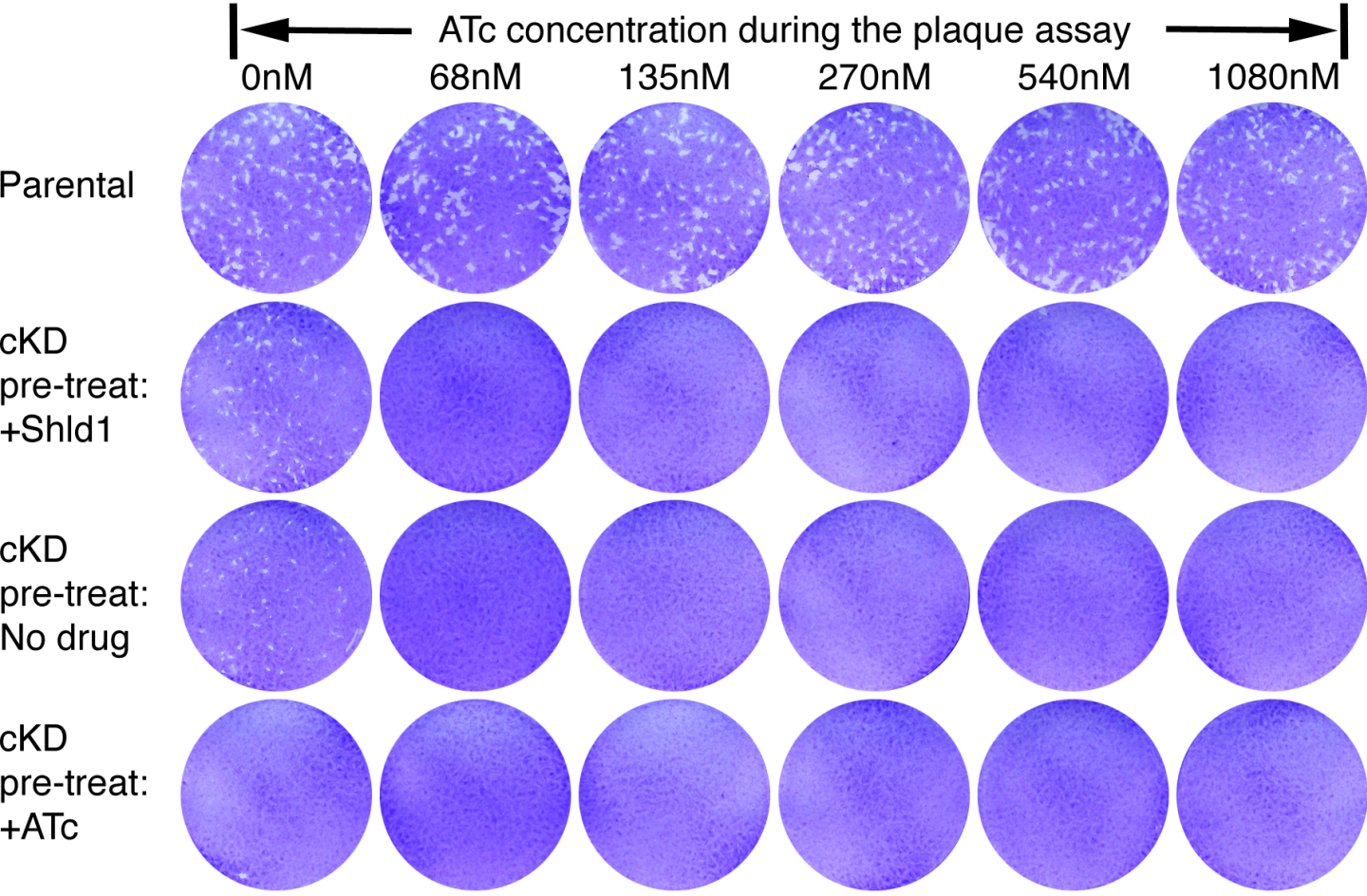

"pre-treat": pre-treated for ~48 h with Shield-1 (Shld1), no drug, or ATc prior to the plaque assay

Figure 5

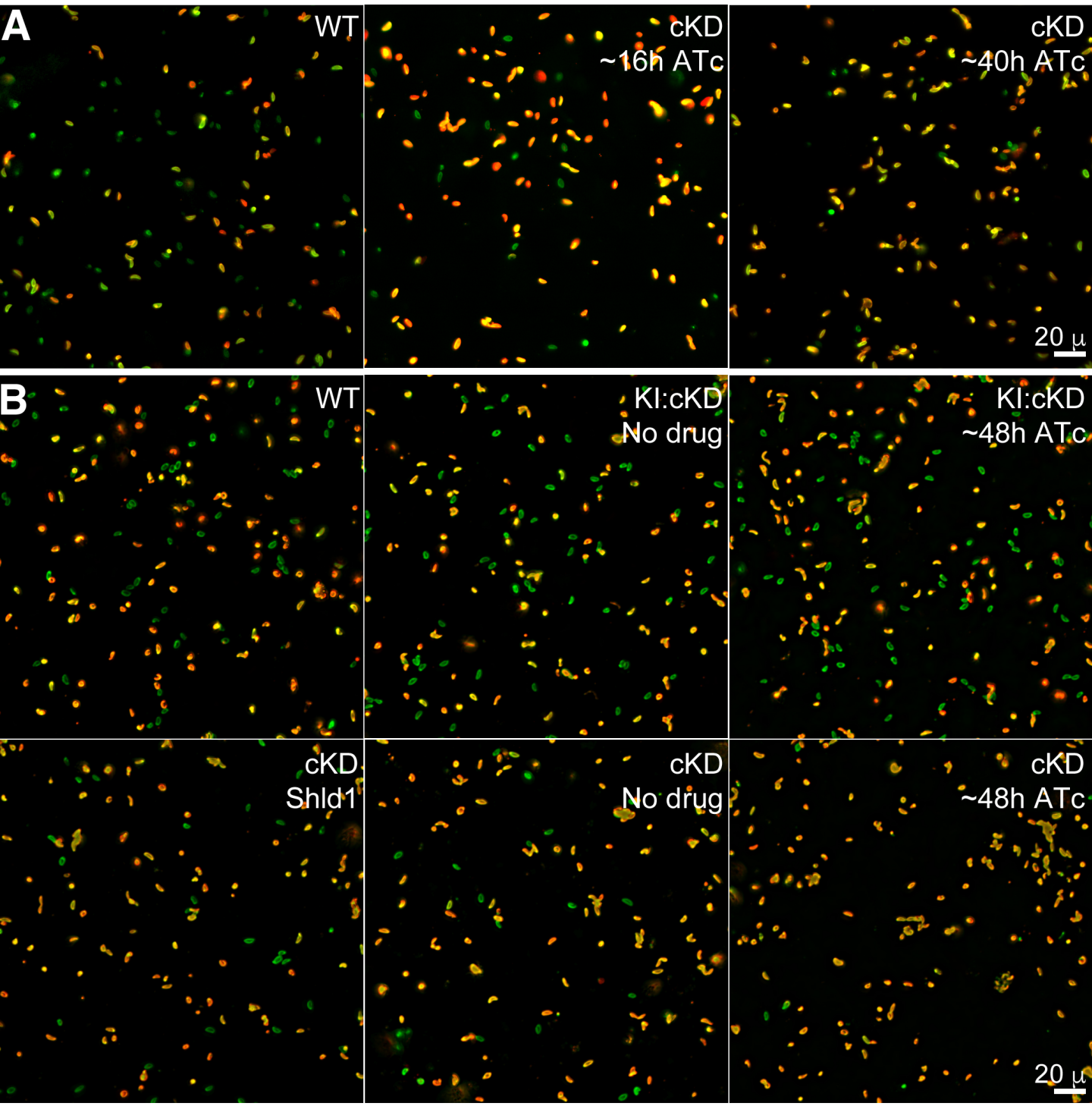
A
WT
cKD
~16h ATc
cKD
~40h ATc
20 μ
B
WT
KI:cKD
No drug
KI:cKD
~48h ATc
cKD
Shld1
cKD
No drug
cKD
~48h ATc
20 μ

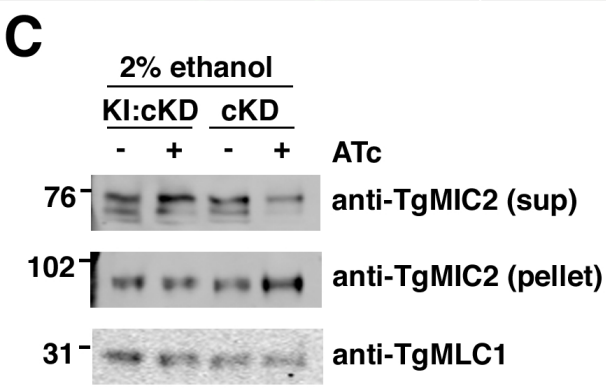
C
2% ethanol
KI:cKD
cKD
- + - +
ATc
76
anti-TgMIC2 (sup)
102
anti-TgMIC2 (pellet)
31
anti-TgMLC1

Figure 6

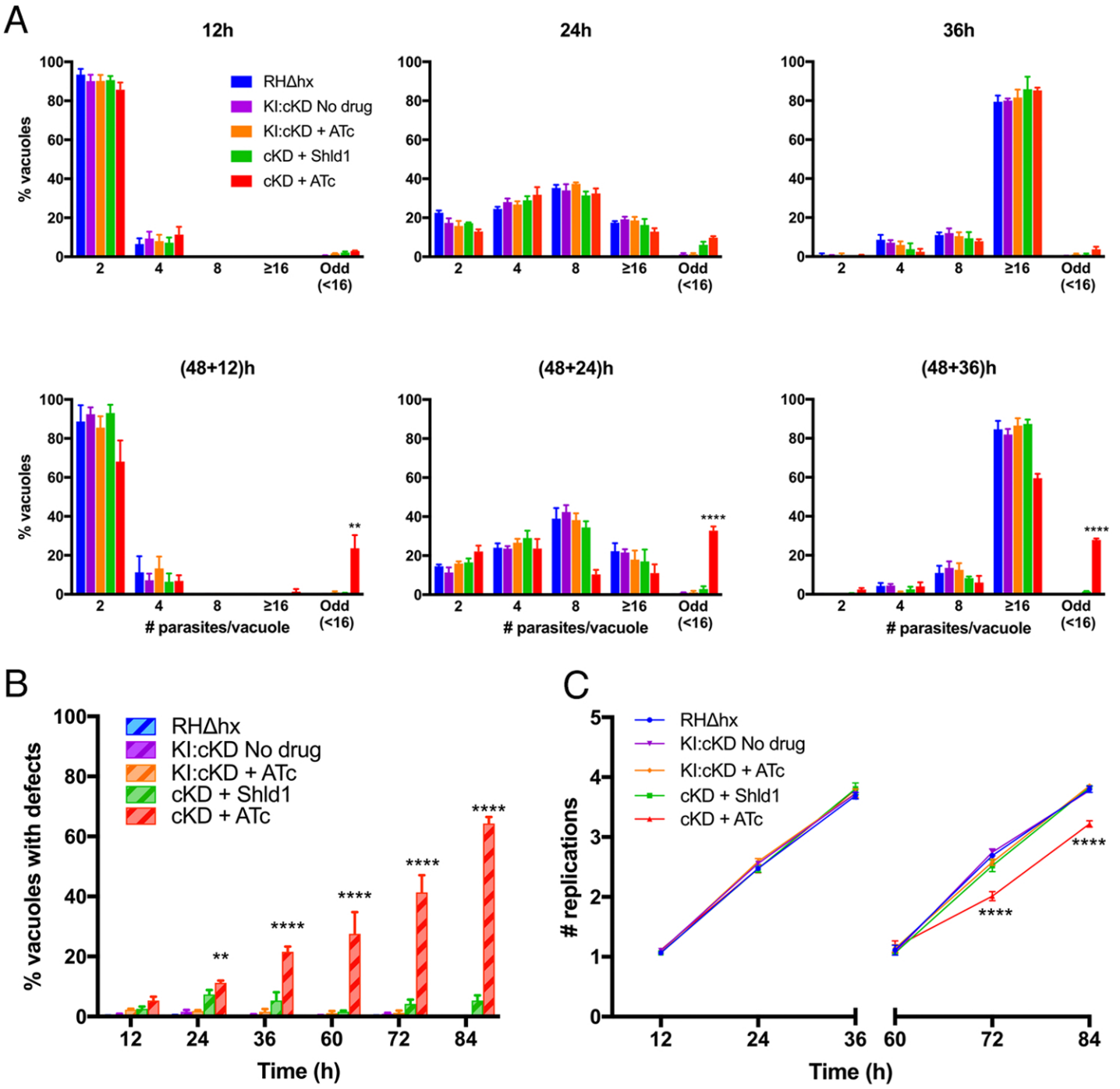
A
12h
24h
36h
(48+12)h
(48+24)h
(48+36)h
% vacuoles
# parasites/vacuole
2
4
8
≥16
Odd (<16)
RHΔhx
KI:cKD No drug
KI:cKD + ATc
cKD + Shld1
cKD + ATc
**
****
B
% vacuoles with defects
Time (h)
C
replications
Time (h)

Figure 7

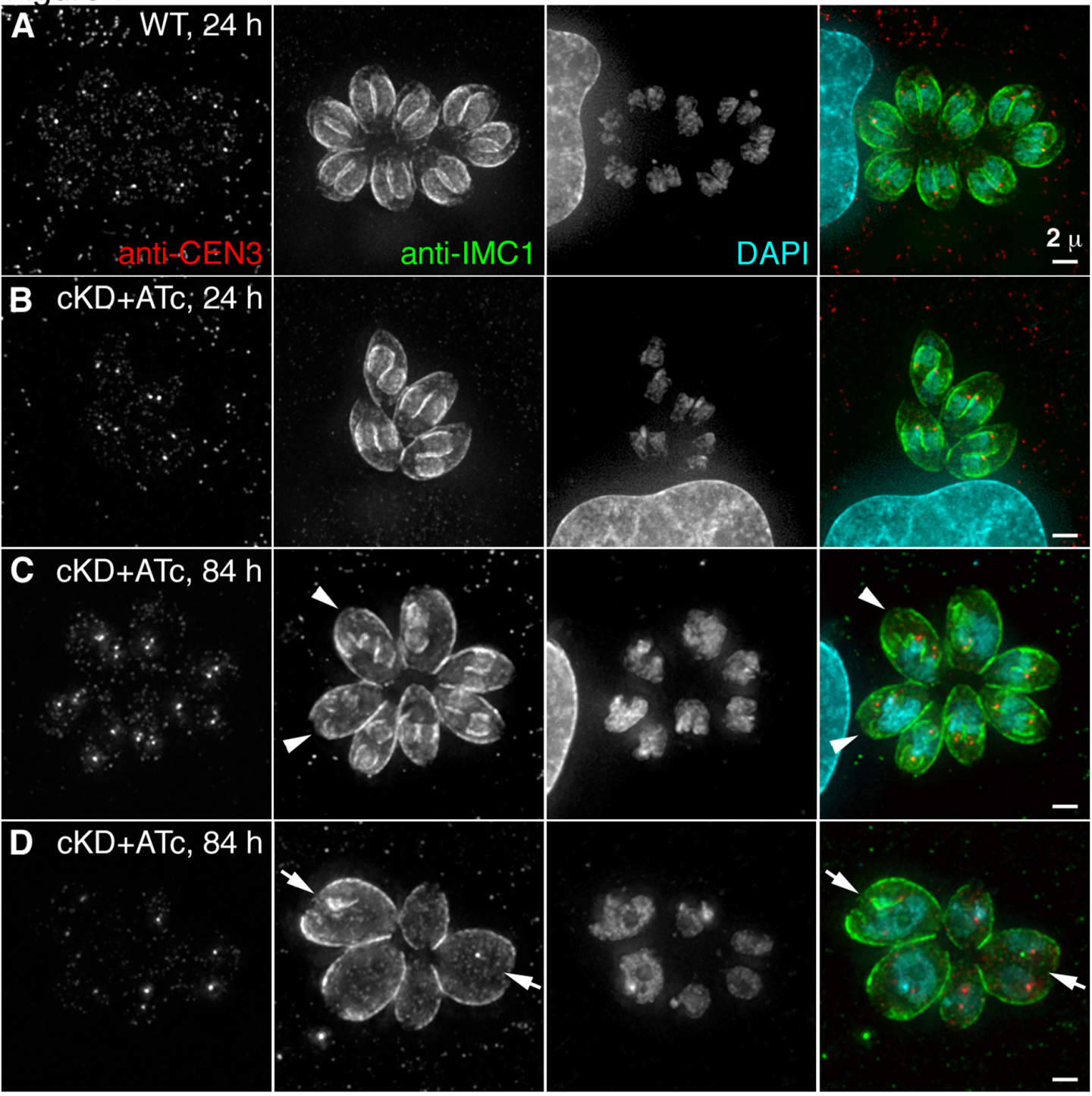
A
WT, 24 h
anti-CEN3
anti-IMC1
DAPI
2 μ
B
cKD+ATc, 24 h
C
cKD+ATc, 84 h
D
cKD+ATc, 84 h